


Influence of different disorder types on Aharonov-Bohm caging in the diamond chainGoran Gligorić¹, Daniel Leykam,² and Aleksandra Maluckov¹¹*P*Group, Vinča Institute of Nuclear Sciences, University of Belgrade, P.O. Box 522, 11001 Belgrade, Serbia*²*Center for Theoretical Physics of Complex Systems, Institute for Basic Science, Daejeon 34126, Republic of Korea* (Received 16 September 2019; revised manuscript received 17 December 2019; accepted 31 January 2020; published 27 February 2020)

The linear diamond chain with fine-tuned effective magnetic flux has a completely flat energy spectrum and compactly localized eigenmodes, forming an Aharonov-Bohm cage. We study numerically how this localization is affected by different types of disorder (static and time-evolving) relevant to recent realizations of Aharonov-Bohm cages in periodically modulated optical waveguide arrays. We demonstrate robustness of localization under static and time-periodic disorder. In contrast, nonquenched (time-dependent) disorder leads to wave-packet spreading and delocalization.

DOI: [10.1103/PhysRevA.101.023839](https://doi.org/10.1103/PhysRevA.101.023839)**I. INTRODUCTION**

The fundamental phenomenon of wave localization can arise from a variety of sources. In nonlinear media, modulational instability leads to localization in the form of wave self-trapping and solitons [1,2]. In linear media, time-independent quenched disorder (QD) induces localization via interference effects in a process known as Anderson localization [3,4]. By contrast, randomly time-evolving nonquenched disorder (NQD) can result in delocalization and enhanced wave transport [5–7]. Linear localization even without disorder occurs in certain periodic structures known as flatband (FB) networks [8–11]. In the FB networks perfectly localized compact modes arise due to the lattice geometry enabling destructive interference between different propagation paths [12,13]. One of the most intriguing questions is to understand the interplay between these different localization mechanisms [14–16]. For example, the combination of nonlinearity and disorder induces delocalization and subdiffusive wave spreading via nonlinear interactions between Anderson-localized linear modes [14].

In the case of FB networks QD transforms the compact modes into Anderson-localized modes with exponential tails [17]. Statistical properties of the localized modes are sensitive to the location of the FBs within the lattice Bloch wave spectrum. For example, when FBs coexist at the same energy as other nonflat (dispersive) bands, Fano resonance-like interaction between the bands leads to “heavy-tailed” statistics in which the mode localization is chiefly determined by rare realizations of the disorder [18] and the FB states acquire a finite lifetime [19]. On the other hand, spectrally isolated FBs typically exhibit strong localization insensitive to the precise strength or profile of the QD, whether on-site (local disorder) describing randomness in the site energies or inter-site (hopping) disorder [18].

In this article we study the influence of various forms of disorder on localization in a particular FB network: the one-dimensional Aharonov-Bohm (AB) cage [20,21]. AB cages are peculiar structures in which all of the spectral

bands are perfectly flat. Originally generated by applying a strong magnetic field to superconducting wire networks [22], more recently AB cages were realized as photonic waveguide arrays by generating an effective magnetic flux using periodic modulation of the waveguides along the propagation axis [23–28]. This longitudinal modulation is analogous to the time-dependent modulation of quantum particles described by the Schrödinger equation, and therefore we consider both static and time-dependent sources of disorder. Disorder can evolve periodically (forming a variant of QD) or nonperiodically in time (standard meaning of the NQD). The compact mode behavior in such cases has not been explored before. These two cases are also intriguing because the mathematical interpretation of localization requires consideration of the time-dependent Hamiltonians, which is usually not the case with respect to the Anderson localization. The main question we are interested in is whether the time-dependent disorder can lead to delocalization, as is the case for regular (non-FB) lattices [5,6].

We model periodically evolving disorder by assuming an initial QD profile has a sinusoidal time dependence [Eq. (2)]. To obtain nonperiodic disorder we randomly change the phase of this sinusoidal modulation at regular time intervals. We find numerically that periodic QD leads to similar strong localization to the standard QD, which can be understood in terms of localized Floquet eigenstates. On the other hand, nonperiodic disorder leads to delocalization, even in this extreme limit where all bands are perfectly flat.

The outline of the paper is as follows. In Sec. II we make a brief overview of the studied phenomena and establish corresponding mathematical model and the methods of numerical analysis. We then study the time evolution of a compact mode excitation in the presence of different disorder types. Section III reviews the case of static disorder, which does not disrupt the strong localization of the eigenstates. We find the chain is more sensitive to hopping disorder than the on-site disorder. Section IV analyzes the case of periodically evolving disorder, and Sec. V discusses the NQD. The concluding Sec. VI summarizes our main findings.

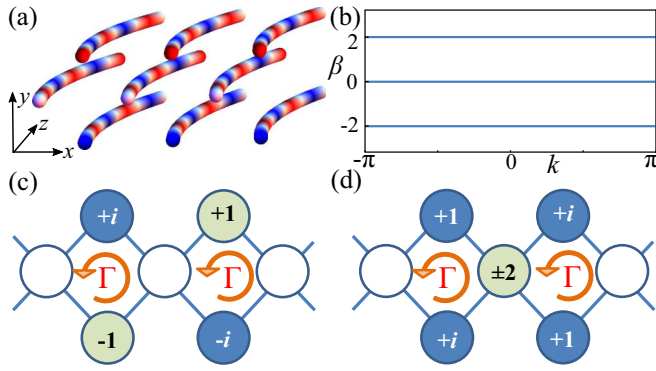


FIG. 1. (a) Schematic of optical waveguide array with effective magnetic flux implemented via periodic modulation of the waveguide depths (shown in red and blue) combined with transverse acceleration of the waveguide positions. (b) Band structure of the array in the Aharonov-Bohm (AB) cage limit $\Gamma = \pi$. (c,d) Schematic of the compactly localized flat band modes: (c) Geometry-induced $\beta_{\text{FB}} = 0$ flat band, and (d) $\beta_{\text{FB}} = \pm 2$ flat bands emerging due to the AB caging.

II. MODEL AND METHODS

AB caging was first studied by the authors of Ref. [21] for tight-binding electrons in certain two-dimensional lattices and quasi-one-dimensional lattices, including the diamond chain. The perfectly flat spectrum arises from destructive interference among different hopping paths at a critical value of the magnetic flux. AB caging was experimentally demonstrated in superconducting wire networks [22], mesoscopic semiconductor lattices [29], arrays of Josephson junctions [30], and properly designed waveguide arrays [27,28].

To investigate phenomenon of the wave mode spreading in the systems with AB cage, we study the light propagation through the periodic diamond chain of coupled optical waveguides in the presence of an artificial gauge field induced by periodically modulating the waveguides, Fig. 1(a). The waveguide arrays are a common playground for simulation of diverse phenomena in condensed matter physics due to easy manipulation with their parameters in the experiments [23–28].

Following the procedure presented in Ref. [23], we model the evolution of slowly varying optical field amplitudes in the waveguides (a_n, b_n, c_n) as

$$\begin{aligned} i \frac{da_n}{dz} &= \kappa (b_n e^{-i\Gamma_{bn}/2} + b_{n-1} + c_n + c_{n-1} e^{-i\Gamma_{cn}/2}) \\ &\quad + \epsilon_{an} a_n, \\ i \frac{db_n}{dz} &= \kappa (a_n e^{i\Gamma_{bn}/2} + a_{n+1}) + \epsilon_{bn} b_n, \\ i \frac{dc_n}{dz} &= \kappa (a_n + a_{n+1} e^{i\Gamma_{cn+1}/2}) + \epsilon_{cn} c_n, \end{aligned} \quad (1)$$

where $n = 1, \dots, N$ indexes the cells, Γ_n is the effective magnetic flux in each plaquette, and κ is the coupling coefficient [15,23], which we normalize to 1 without loss of generality. These equations are obtained by averaging over high-frequency modulation in z and can thus host both QDs and NQDs.

The ϵ_{jn} terms in Eq. (1) describe the on-site disorder potential, which we model as [31]

$$\epsilon_{jn} = \epsilon_{jn}^{\text{QD}} + \epsilon_{jn}^{\text{ED}}(z) = \epsilon_{jn}^{(0)} \{1 + A \sin[\omega_0 z + \phi_{jn}(z)]\}, \quad (2)$$

where $j = a, b, c$ is the sublattice index. The term $\epsilon_{jn}^{\text{QD}} \equiv \epsilon_{jn}^{(0)}$ describes the on-site static disorder, while $\epsilon_{jn}^{\text{ED}}(z)$ describes the on-site evolving disorder. We take $\epsilon_{jn}^{(0)}$ to be uncorrelated random numbers from the interval $[-W/2, W/2]$, where the parameter W is the disorder strength. The time-evolving disorder term is characterized by amplitude A , frequency $\omega_0 = 2\pi/Z_0$, and the phase terms $\phi_{jn}(z)$.

Meanwhile, we model hopping disorder as fluctuations in the hopping phase determining the effective magnetic flux

$$\Gamma_{jn} = \Gamma_0 [1 + \delta\Gamma_{jn}(z)]. \quad (3)$$

The last term $\delta\Gamma_{jn}(z)$ takes a similar form to $\epsilon_{jn}(z)$, being separated into static and z -dependent terms. The small fluctuations of the magnetic flux resemble the experimental uncertainties in preparing the external artificial magnetic field.

We further distinguish the evolving part of the disorder into two different classes: whether it evolves periodically or nonperiodically in z . The latter models NQD, which can be interpreted as an uncorrelated thermally induced disorder in the context of electronic systems. To create NQD with controllable rate of change in z , we follow the approach of the authors of Ref. [32] and consider noise in the modulation phase $\phi_{jn}(z)$. After a fixed step length, named the dephasing length Δz , we randomly reassign the modulation phases $\phi_{jn}(z)$, drawn uniformly from the interval $[-\pi, \pi]$.

The eigenvalue spectrum of the diamond chain with artificial flux Γ in the absence of disorder consists of three bands:

$$\beta_{\text{FB}} = 0, \quad \beta_{\pm} = \pm 2\kappa \sqrt{1 + \cos(\Gamma/2) \cos(k)}. \quad (4)$$

One band is always independent of the normalized wave number k , forming a dispersionless FB, while the other k -dependent bands are dispersive (DBs). The FB is a consequence of diamond chain geometry. Depending on the value of Γ three different cases are possible: one FB touching two DBs ($\Gamma = 0, 2\pi$), one gapped FB ($\Gamma \neq 0, \pi, 2\pi$), three distinct FBs ($\Gamma = \pi$), the last forming an AB cage, with completely flat spectrum shown in Fig. 1(b).

In a chain with N unit cells each FB has an N -fold degeneracy in the absence of disorder. The propagation dynamics of localized excitations in this case can be intuitively understood in terms of a basis of N compact, and in general, nonorthogonal localized states (CLSs). These states can be expressed as a superposition of the more familiar delocalized Bloch wave eigenmodes. The CLSs for the diamond chain are illustrated schematically in Figs. 1(c) and 1(d). These CLS field amplitudes are obtained by seeking propagation-invariant solutions of Eq. (1) that only excite a finite number of lattice sites. One can verify that diffraction to neighboring unoccupied lattice sites is completely inhibited by destructive interference between the upper and lower legs of the chain. This is the mechanism responsible for the flatband localization. In the AB cage limit an arbitrary excitation of the lattice can be expressed as a superposition of CLS from the three

flatbands with energies $\beta = 0, \pm 2$, such that the propagation dynamics will be strictly periodic.

In this work we focus on the investigation of the disorder impact on the diamond chain with fulfilled conditions for AB caging. Therefore, we will consider the dynamics of isolated compact modes from the different flatbands: CLS from $\beta_{\text{FB}} = 0$ and CLS from $\beta_{\text{FB}} = \pm 2$. We will also briefly comment in Sec. VI on the behavior of single site excitations, where a site a or site b from the central lattice cell is initially excited.

To characterize the dynamics of a wave packet and their localization, it is useful to consider the following quantities: the total intensity in each unit cell I_n , the second moment m_2 , the participation ratio PR, and the imbalance η . Assuming all wave packets are normalized such that $\sum_n I_n = 1$, these quantities are defined as

$$\begin{aligned}
 I_n(z) &= |a_n(z)|^2 + |b_n(z)|^2 + |c_n(z)|^2, \\
 m_1(z) &= \sum_n \left\{ n|a_n(z)|^2 + \left(n + \frac{1}{2}\right)[|b_n(z)|^2 + |c_n(z)|^2] \right\}, \\
 m_2(z) &= \sum_n \left\{ (n - m_1(z))^2 |a_n(z)|^2 \right. \\
 &\quad \left. + \left(n + \frac{1}{2} - m_1(z)\right)^2 [|b_n(z)|^2 + |c_n(z)|^2] \right\}, \\
 PR(z) &= \left(\sum_n I_n^2 \right)^{-1}, \\
 \eta(z) &= \sum_n [|a_n(z)|^2 - |b_n(z)|^2 - |c_n(z)|^2],
 \end{aligned}$$

where $\psi_n(z) = [a_n(z), b_n(z), c_n(z)]^T$ and $m_1(z)$ is the first moment or center of mass. The distribution of I_n over the lattice cells shows the efficiency of certain disorder which is expected mostly to affect the tails of the initially excited compact modes. m_2 gives information about the CLS or wave-packet density spreading, PR about the number of sites significantly populated by the field, while the imbalance η about how energy is distributed between corresponding sublattices. Although the second moment and the participation ratio are linked, and broader wave packets are expected to occupy a greater number of sites, there are some particular situations in which this is not so. For example, in the case with self-trapping (nonlinear networks) the second moment typically increases in time (due to unbounded spreading of linear dispersive waves), but the participation number stays more or less constant. It is related to a frozen bulk that does not evolve with certain sites remaining highly occupied. When the noise is added to such a system the interplay between the self-trapping and (de)localization from disorder includes interesting features [33].

III. STATIC DISORDER

We begin by briefly reviewing the effect of static disorder on the diamond chain, which was previously investigated by the authors of Refs. [18,21,34]. In one-dimensional discrete lattices static uncorrelated disorder typically induces

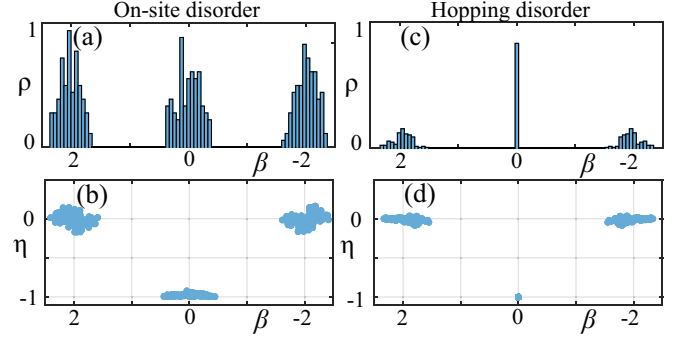


FIG. 2. The (a) eigenstate density spectrum ρ and (b) corresponding imbalance η for diamond chain with $\Gamma = \pi$ (AB cage limit) in the presence of on-site static disorder of strength $W = 1$. (c,d) The corresponding quantities in the presence of static hopping disorder are plotted.

Anderson localization with eigenstate profiles becoming exponentially localized $\sim e^{-|n|/\xi}$, where ξ is the localization length [4]. The ξ is also the characteristic length an initially localized excitation of the lattice can spread [14]. It scales as $\xi \propto v_g^2/W^2$ in the limit of weak disorder strength W , where v_g is the wave-group velocity in the absence of disorder.

The characteristic scaling of ξ does not occur in flatbands because $v_g = 0$. Instead, the eigenmode spreading becomes sensitive to gap Δ separating the FB from other DBs [18]. When $W \lesssim \Delta$ there is strong mixing between the states within the FB, which hybridize and lift their degeneracy. In addition, mixing between the FB and evanescent modes derived from the other dispersive bands results in a localization length determined by band gap Δ rather than the disorder strength W . Thus, for small W the degree of localization becomes independent of W . Once $W \gtrsim \Delta$, strong mixing between the flat and dispersive bands dominates over the details of the lattice band structure and conventional Anderson localization (sensitive to W) is expected to emerge [18]. On the other hand, if the disorder potential has some local symmetry that inhibits mixing with FB states they will preserve their compact localization.

In the following we consider two types of static disorder ($A = 0$):

- (1) On-site disorder ($\epsilon_{jn} \neq 0, \delta\Gamma_{jn} = 0$);
- (2) Hopping disorder ($\epsilon_{jn} = 0, \delta\Gamma_{jn} \neq 0$).

To demonstrate the differing effects of these two disorder types we solve the eigenvalue problem numerically to obtain the eigenstate spectra shown in Fig. 2, using a lattice with $N = 101$ cells and disorder strength $W = 1$. Without disorder the three isolated FBs are N -fold degenerate. Introducing quenched disorder lifts the degeneracy. The on-site disorder fully removes the degeneracy, i.e., all FBs are affected [Fig. 2(a)], and the sublattice symmetry of the eigenstates is broken, leading to $\eta \neq 0, -1$ [Fig. 2(b)]. On the other hand, the hopping disorder only partially lifts the degeneracy of the FBs: The degeneracy of the two periphery FBs ($\beta_{\text{FB}} = \pm 2$) is removed, but the central FB remains degenerate and its eigenstates preserve their sublattice symmetry [Figs. 2(c) and 2(d)]. This is because the central FB is protected by the lattice's bipartite symmetry, which is preserved under the hopping disorder.

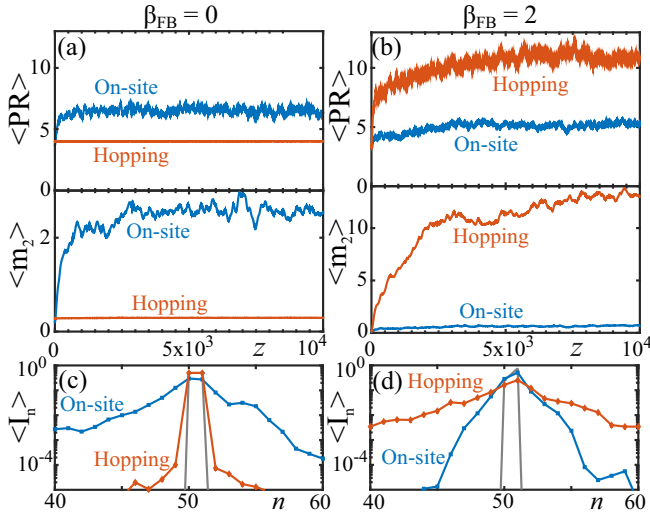


FIG. 3. (a,b) Dynamics of the disorder-averaged participation ratio $\langle PR \rangle$ and second moment $\langle m_2 \rangle$ obtained for excitations of the (a) $\beta_{FB} = 0$ and (b) $\beta_{FB} = 2$ CLS. (c,d) Disorder-averaged intensity profiles $\langle I_n \rangle$ at $z = 10^4$ for (c) $\beta_{FB} = 0$ and (d) $\beta_{FB} = 2$ CLS excitations. Averages are obtained over 50 disorder realizations.

Next we study the impact of the disorder on the propagation dynamics in the AB cage by numerically solving Eq. (1), taking the normalized compact modes of Figs. 1(c) and 1(d) as initial conditions. We fix the disorder strength $W = 1$ and consider an ensemble of 50 disorder realizations. Figures 3(a) and 3(b) illustrate the dynamics of the disorder-averages $\langle PR \rangle$ and $\langle m_2 \rangle$, which saturate to finite values, indicating the onset of Anderson localization. Figures 3(c) and 3(d) show the ensemble-averaged beam intensity profile $\langle I_n \rangle$ after a propagation distance of $z = 10^4$. Consistently with the numerically calculated eigenvalue spectra, we observe that the compact localization present in the ideal (nondisordered) system is destroyed, and replaced by exponential Anderson localization. The $\beta_{FB} = 0$ CLS is much less sensitive to the hopping disorder, which does not spread at all and essentially preserves its initial beam profile.

Figure 4 quantifies the dependence of the long time localization measures $\langle PR \rangle$ and $\langle m_2 \rangle$ on the disorder strength W . For very weak disorder ($W < 0.01$) $\langle PR \rangle$ and $\langle m_2 \rangle$ of initially injected CLS from $\beta_{FB} = 0$ are saturated to the corresponding values in the absence of disorder. This is the case for both on-site and hopping disorder. While this tendency continues for the hopping disorder for stronger W , the on-site disorder starts to affect the CLS from $\beta_{FB} = 0$, which is slightly smeared over the neighboring cells, corresponding to saturation of $\langle PR \rangle$ and $\langle m_2 \rangle$ at higher values. For strong disorder $W \gtrsim 2$ we observe an increase in the spreading due to a transition from AB cage-induced localization to regular Anderson localization.

IV. PERIODIC DISORDER

The evolution of periodically driven systems can be understood using the Floquet formalism, in which one considers

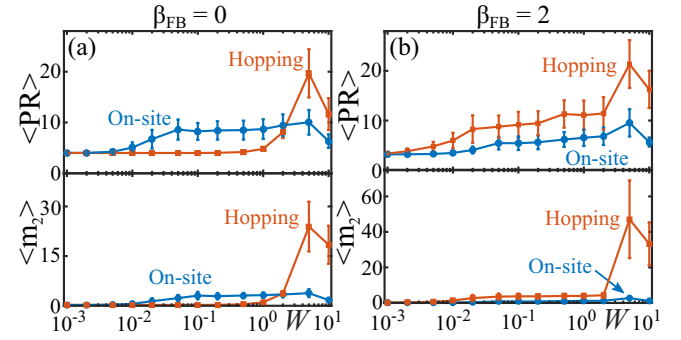


FIG. 4. Disorder-averaged $\langle PR \rangle$ (upper plot) and $\langle m_2 \rangle$ (lower plot) after propagation length $z = 10^3$ for different stationary QD realizations vs. disorder strength W . (a) CLS from central FB ($\beta_{FB} = 0$) and (b) CLS from the periphery FB are initially excited in the lattice (from $\beta_{FB} = 2$). Error bars illustrate the standard deviations of corresponding quantities.

the field profile at integer multiples of the driving period Z_0 [35,36]. This is described by the unitary evolution operator $U(Z_0) = \exp[\int_0^{Z_0} H(z) dz]$, where $H(z)$ is the time-dependent Hamiltonian governing the dynamics. Using the bra-ket notation the field evolves as

$$|\psi_n(z + Z_0)\rangle = U|\psi_n(z)\rangle, \quad |\psi_n(z)\rangle = \begin{pmatrix} a_n(z) \\ b_n(z) \\ c_n(z) \end{pmatrix}. \quad (5)$$

The stroboscopic dynamics can be understood via projection of any initial state onto the eigenmodes of this Floquet evolution operator. In particular, the eigenstates of U correspond to the eigenstates of a static effective Floquet Hamiltonian $H_{\text{eff}} = i \log(U)/Z_0$. This allows interpretation of the periodically disordered system dynamics in a similar manner to that of the static disorder case. We obtain the Floquet eigenmodes by computing the individual matrix elements of U using numerical beam propagation over one driving period, and then numerically diagonalizing the resulting $N \times N$ unitary matrix (see Refs. [35,36] for details).

For periodically evolving disorder an important new energy scale emerges: the ratio of the characteristic frequency of the disorder $\omega_0 = 2\pi/Z_0$ to the gap size Δ . When ω_0 is resonant with one of the gap sizes there can be strong mixing between the eigenstates of the static system to form qualitatively different Floquet eigenstates. To explore the influence of ω_0 on the wave-packet spreading in the disordered system we consider three different classes of periodic disorder (taking $A = 1$):

- (1) driving resonant with the band gap ($\omega_0 = 2$);
- (2) off-resonant driving ($\omega_0 = 0.1$);
- (3) doubly resonant driving ($\omega_0 = 4$).

In particular, the resonant and doubly resonant driving cases can induce strong mixing between different elementary CLSs to create new Floquet eigenstates. We will consider both on-site and hopping disorders in the following.

First, we calculated the Floquet eigenmode spectrum under these different classes of periodic disorder. Regardless of Z_0 , we obtain localized eigenmodes, indicating the persistence of the Anderson localization under periodic driving. Similar to

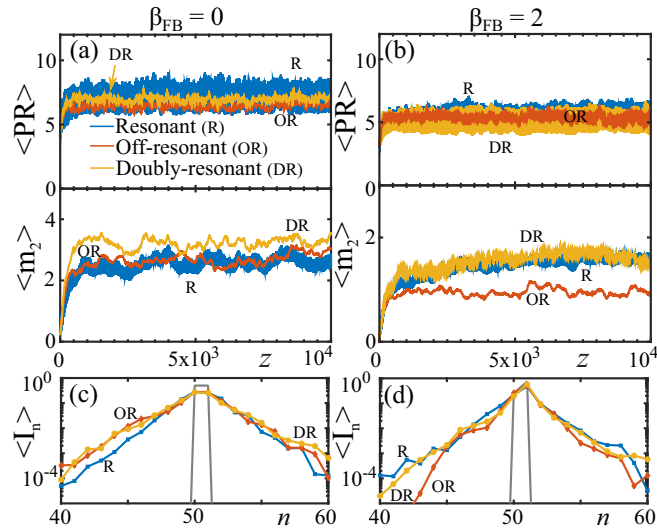


FIG. 5. Dynamics of the disorder-averaged participation ratio (PR) and second moment $\langle m_2 \rangle$ obtained for excitations of the (a) $\beta_{\text{FB}} = 0$ and (b) $\beta_{\text{FB}} = 2$ CLS. (c,d) Intensity profiles $\langle I_n \rangle$ at $z = 10000$ for (a) $\beta_{\text{FB}} = 0$ and (b) $\beta_{\text{FB}} = 2$ CLS excitations. Averages are obtained over 50 realizations of on-site disorders.

the eigenvalues of the static case shown in Fig. 2, the on-site disorder affects all FBs, while hopping disorder preserves the degeneracy of the zero energy FB.

Figures 5(a) and 5(b) shows the long time dynamics of the disorder-averaged participation number $\langle \text{PR} \rangle$ and the second moment $\langle m_2 \rangle$ for the on-site periodic disorder. Both $\langle \text{PR} \rangle$ and $\langle m_2 \rangle$ saturate after an initial transient spreading, regardless of the type of disorder frequency or the initial CLS. Localization after that persists. When there are resonances, additional rapid oscillations in $\langle \text{PR} \rangle$ and $\langle m_2 \rangle$ appear due to interband coupling; this occurs for the resonant driving when the central FB is initially excited, and for both resonant and doubly resonant driving when one of the peripheral FBs is excited. The averaged intensity profiles in Figs. 5(c) and 5(d) show similar exponential tails in all cases.

We can understand the effect of the periodic disorder on the wave-packet spreading following the approach in Refs. [31,32]. Based on perturbation theory for linear systems in the presence of time-dependent perturbations, we expect to see transitions between different static eigenstates. The strength of these transitions is determined by the spatial overlap between the states, and whether the frequency of the perturbation is resonant with the energy difference between the states. Due to the strong localization induced by the AB caging, there can only be appreciable overlap with directly neighboring CLS, which have random energies due to the static part of the disorder. Consequently, while resonances between neighboring states can, in principle, lead to slight expansion of the wavepacket, this occurs with low probability. Therefore the wave packets remain bounded and strongly localized. The described findings are clearly seen in Fig. 6 where the effect of periodic QDs of different strength on the CLS spreading is presented. In general, slowly increasing slopes of the curves $\langle \text{PR} \rangle$ versus W and $\langle m_2 \rangle$ versus W are

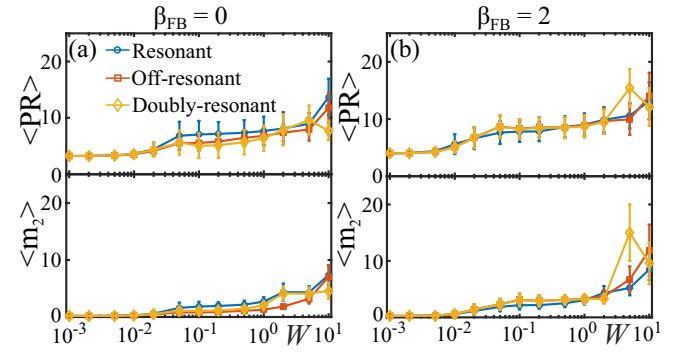


FIG. 6. The averaged value of $\langle \text{PR} \rangle$ (upper plot) and $\langle m_2 \rangle$ (lower plot) over the propagation length $z = 1000$ for different stationary QD realizations vs. disorder strength W . (a) CLS from central FB ($\beta_{\text{FB}} = 0$) and (b) CLS from the periphery FB ($\beta_{\text{FB}} = 2$) are initially excited in the lattice.

consequences of the time dynamics caused by the periodic modulation of on-site disorder.

The corresponding results for time-periodic hopping disorder are shown in Fig. 7, which illustrates the evolution of the disorder-averaged PR, m_2 , and intensity profiles I_n for both types of the compact localized modes. In this case the dynamics of the $\beta_{\text{FB}} = 0$ FB shows a clear difference between the resonant driving and the off-resonant and doubly resonant drivings: The resonant driving induces exponential tails in the localized mode, the others preserve the strong localization of the $\beta_{\text{FB}} = 0$ CLS, which remains almost compact. This is a straightforward consequence of the wave packets' relaxation via the bottleneck path through the a sublattice in the resonant case. Regarding the CLS initiated from the $\beta_{\text{FB}} = 2$, all types of modulated hopping disorder induced the fast growth and saturation of $\langle \text{PR} \rangle$ and $\langle m_2 \rangle$ to finite values

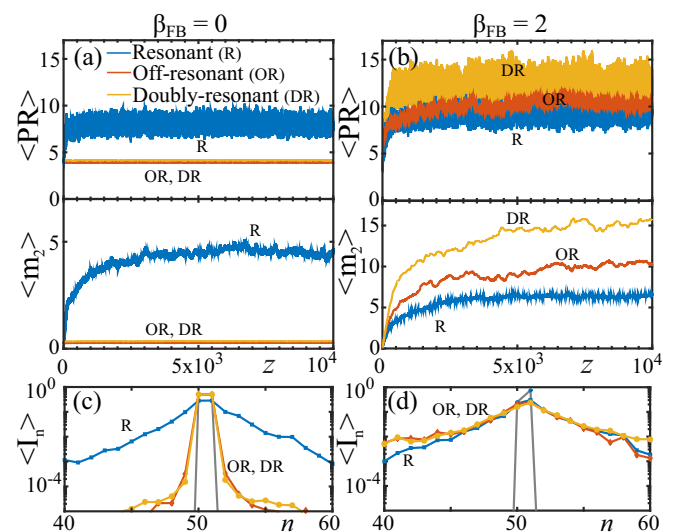


FIG. 7. Dynamics of the disorder-averaged participation ratio $\langle \text{PR} \rangle$ and second moment $\langle m_2 \rangle$ obtained for excitations of the (a) $\beta_{\text{FB}} = 0$ and (b) $\beta_{\text{FB}} = 2$ CLS. (c,d) Intensity profiles $\langle I_n \rangle$ at (c) $z = 10000$ for $\beta_{\text{FB}} = 0$ and (d) $\beta_{\text{FB}} = 2$ CLS excitations. Averages are obtained over 50 realizations of hopping disorders.

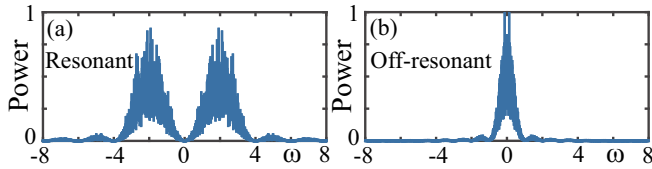


FIG. 8. The on-site NQD power spectra obtained after averaging over ten different realizations of the set of random numbers for (a) resonant NQD and (b) off-resonant NQD.

[Fig. 7(b)] and the exponential localization [Fig. 7(d)]. Again the observed dynamical properties can be associated with the active role of the a sublattice, which is in this case generically whole time “populated” and thus “introduced” in the mode relaxation.

V. NONQUENCHED DISORDER

Finally, we study the nonquenched disorder (NQD), which introduces an additional characteristic scale: the dephasing length Δz . The monochromatic perturbations studied in the previous section are now broadened to have a finite bandwidth, enabling coupling between successive CLS and wave-packet spreading. The efficiency of the spreading is dictated by the NQD power spectrum, shown in Fig. 8 for the two different types of NQD we will consider (with amplitude $A = 1$):

- (1) Resonant NQD $\omega_0 = 2$, $\Delta z = 5$;
- (2) Off-resonant NQD $\omega_0 = 0.1$, $\Delta z = 10$.

The NQD is characterized by abrupt changes of the disorder realization along the propagation directions which occur at regular distances. This results in momentum “kicks” which can induce spreading of the wave packet. For example, in regular (non-FB) lattices the evolving disorder results in superdiffusive wave-packet spreading [5–7].

Figure 9 illustrates the wave-packet spreading under representative examples of the NQD, measured via the averaged

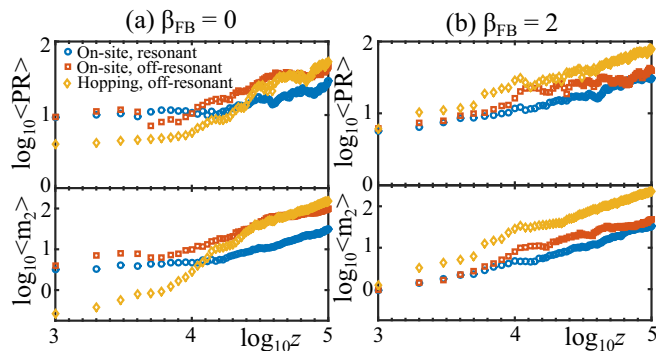


FIG. 9. Averaged values of participation ratio (PR) and second moment $\langle m_2 \rangle$ over 50 propagation windows, which are obtained for CLS from (a) $\beta_{\text{FB}} = 0$ excitation and (b) the CLS from $\beta_{\text{FB}} = 2$ excitation and different types of NQDs are shown in log-scale. The mentioned propagation windows are obtained by dividing the total propagation length into 50 parts of equal length.

participation number (PR) and the second moment $\langle m_2 \rangle$. Both quantities grow with z , regardless of the type of NQD or CLS excitation. This indicates that NQD breaks localization and causes wave-packet spreading in all cases, similar to regular lattices. Comparing $\langle \text{PR} \rangle$ and $\langle m_2 \rangle$, we find faster spreading for off-resonant hopping disorder than in the cases with on-site disorder. This difference is stronger for CLS from $\beta_{\text{FB}} = 2$ than CLS from $\beta_{\text{FB}} = 0$ excitation. Additionally, the rate of spreading measured by $\langle m_2 \rangle$ for the on-site disorders tends to slow after an initial transient, but not in the case of hopping disorder. Furthermore, for the CLS from $\beta_{\text{FB}} = 0$ excitation faster spreading occurs for off-resonant disorder compared to the resonant case, which we attribute to the stronger overlap of the disorder spectrum with the static modes. We quantify the destruction of localization via NQD by estimating the slopes (α) of curves $\log(\langle m_2(z) \rangle)$ versus $\log(z)$ for each of CLSs in Fig. 9. The most effective hopping NQD is characterized by power-law spreading $\alpha \approx 1.5$ for CLS0 and $\alpha \approx 1$ for CLS2, corresponding to superdiffusion and regular diffusion, respectively. The lack of dispersive waves with rapid spreading to media means that the spreading exponents are significantly lower than $\alpha \approx 2.4$ for the case of regular (non-FB) photonic lattices [5–7].

VI. CONCLUSION

The purpose of this study was to reveal the effect of different types of quenched and nonquenched disorders on the dynamics of compact localized excitations (CLSs) in the diamond chain threaded by an effective magnetic flux, which forms an Aharonov-Bohm cage with a completely flat spectrum. These classes of disorder are particularly relevant to recent experimental realizations of AB cages in photonic waveguide arrays [27,28]. We found that the CLS become exponentially localized under quenched and periodic disorders. Notably, strong localization under periodic disorder persists even if the periodic modulation resonantly couples different bands. Abrupt changes of the disorder realization forming nonquenched disorder destroys localization and induces wave-packet spreading for both on-site and hopping disorders, with the last term resulting in more rapid spreading.

We focused on the dynamics of the CLS hosted by the flatbands of the diamond chain. Such CLS are obtained via excitation of multiple waveguides. We found qualitatively similar localization behavior for single waveguide excitations since they can be expressed as superpositions of the CLS. Namely, an a waveguide excitation is a superposition of CLS from the $\beta_{\text{FB}} = \pm 2$ bands, while a b waveguide excitation involves CLS from all the FBs. In both cases the localization or spreading dynamics are accompanied by rapid oscillations due to interference between the different bands.

In the future, it would be interesting to generalize this study to two- and three-dimensional Aharonov-Bohm cage lattices [21], where the dynamics are expected to be more sensitive to the disorder strength. We considered idealized tight-binding models of quenched and nonquenched disorder, which we believe are representative of a variety of disordered systems including waveguide arrays and optical lattices for

cold atoms. To determine the conditions under which the delocalization or saturation of wave-packet spreading may be observable in experiment, it will be necessary to conduct more rigorous simulations taking into account the rapid periodic modulation [27] or auxiliary sites [28] used to create the synthetic magnetic field.

ACKNOWLEDGMENTS

We acknowledge support from the Ministry of Education, Science, and Technological Development of the Republic of Serbia (Project No. III 45010) and the Institute for Basic Science in Korea (IBS-R024-Y1).

-
- [1] R. S. MacKay, L. Vazquez, and M. P. Zorzano, *Localization and Energy Transfer in Nonlinear Systems* (World Scientific Publishing, Singapore, 2003).
- [2] D. K. Campbell, S. Flach, and Yu. S. Kivshar, Localizing energy through nonlinearity and discreteness, *Physics Today* **57**(1), 43 (2004).
- [3] P. W. Anderson, Absence of diffusion in certain random lattices, *Phys. Rev.* **109**, 1492 (1958).
- [4] B. Kramer and A. MacKinnon, Localization: theory and experiment, *Rep. Prog. Phys.* **56**, 1469 (1993).
- [5] L. Levi, Y. Krivolapov, S. Fishman, and M. Segev, Hypertransport of light and stochastic acceleration by evolving disorder, *Nat. Phys.* **8**, 912 (2012).
- [6] Y. Krivolapov, L. Levi, S. Fishman, M. Segev, and M. Wilkinson, Super-diffusion in optical realizations of Anderson localization, *New J. Phys.* **14**, 043047 (2012).
- [7] A. Iomin, Hyperdiffusion of quantum waves in random photonic lattices, *Phys. Rev. E* **92**, 022139 (2015).
- [8] O. V. Kibis, H. Sigurdsson, and I. A. Shelykh, Aharonov-Bohm effect for excitons in a semiconductor quantum ring dressed by circularly polarized light, *Phys. Rev. B* **91**, 235308 (2015).
- [9] M. Hasan, I. V. Iorsh, O. V. Kibis, and I. A. Shelykh, Optically controlled periodical chain of quantum rings, *Phys. Rev. B* **93**, 125401 (2016).
- [10] G. Möller and N. R. Cooper, Synthetic gauge fields for lattices with multi-orbital unit cells: routes towards a π -flux dice lattice with flat bands, *New J. Phys.* **20**, 073025 (2018).
- [11] K. Fang, Z. Yu, and S. Fan, Realizing effective magnetic field for photons by controlling the phase of dynamic modulation, *Nat. Photon.* **6**, 782 (2012).
- [12] D. Leykam, A. Andreanov, and S. Flach, Artificial flat band systems: from lattice models to experiments, *Adv. Phys.: X* **3**, 1473052 (2018).
- [13] D. Leykam and S. Flach, Perspective: Photonic flatbands, *Photon.* **3**, 070901 (2018).
- [14] S. Flach, D. O. Krimmer, and C. Skokos, Universal Spreading of Wave Packets in Disordered Nonlinear Systems, *Phys. Rev. Lett.* **102**, 024101 (2009).
- [15] G. Gligorić, P. P. Beliĉev, D. Leykam, and A. Maluckov, Nonlinear symmetry breaking of Aharonov-Bohm cages, *Phys. Rev. A* **99**, 013826 (2019).
- [16] M. Di Liberto, S. Mukherjee, and N. Goldman, Nonlinear dynamics of Aharonov-Bohm cages, *Phys. Rev. A* **100**, 043829 (2019).
- [17] S. Flach, D. Leykam, J. D. Bodyfelt, P. Matthies, and A. S. Desyatnikov, Detangling flat bands into Fano lattices, *Europhys. Lett.* **105**, 30001 (2014).
- [18] D. Leykam, J. D. Bodyfelt, A. S. Desyatnikov, and S. Flach, Localization of weakly disordered flat band states, *Eur. Phys. J. B* **90**, 1 (2017).
- [19] C. Gneiting, Z. Li, and F. Nori, Lifetime of flatband states, *Phys. Rev. B* **98**, 134203 (2018).
- [20] Y. Aharonov and D. Bohm, Significance of electromagnetic potentials in the quantum theory, *Phys. Rev.* **115**, 485 (1959).
- [21] J. Vidal, R. Mosseri, and B. Douçot, Aharonov-Bohm Cages in Two-Dimensional Structures, *Phys. Rev. Lett.* **81**, 5888 (1998).
- [22] C. C. Abilio, P. Butaud, Th. Fournier, B. Pannetier, J. Vidal, S. Tedesco, and B. Dalzotto, Magnetic Field Induced Localization in a two-dimensional Superconducting Wire Network, *Phys. Rev. Lett.* **83**, 5102 (1999).
- [23] S. Longhi, Aharonov-Bohm photonic cages in waveguide and coupled resonator lattices by synthetic magnetic fields, *Opt. Lett.* **39**, 5892 (2014).
- [24] I. L. Garanovich, S. Longhi, A. A. Sukhorukov, and Yu. S. Kivshar, Light propagation and localization in modulated photonic lattices and waveguides, *Phys. Rep.* **518**, 1 (2012).
- [25] L. Martin, G. Di Giuseppe, A. Perez-Leija, R. Keil, F. Dreisow, M. Heinrich, S. Nolte, A. Szameit, A. F. Abouraddy, D. N. Christodoulides, and B. E. A. Saleh, Anderson localization in optical waveguide arrays with off-diagonal coupling disorder, *Opt. Express* **19**, 13636 (2011).
- [26] S. Longhi, D. Gatti, and G. D. Valle, Non-Hermitian transparency and one-way transport in low-dimensional lattices by an imaginary gauge field, *Phys. Rev. B* **92**, 094204 (2015).
- [27] S. Mukherjee, M. Di Liberto, P. Öhberg, R. R. Thomson, and N. Goldman, Experimental Observation of Aharonov-Bohm Cages in Photonic Lattices, *Phys. Rev. Lett.* **121**, 075502 (2018).
- [28] M. Kremer, I. Petrides, E. Meyer, M. Heinrich, O. Zilberberg, and A. Szameit, Non-quantized square-root topological insulators: a realization in photonic Aharonov-Bohm cages, *Nat. Commun.* **11**, 907 (2020).
- [29] C. Naud, G. Faini, and D. Mailly, Aharonov-Bohm cages in 2D normal Metal Networks, *Phys. Rev. Lett.* **86**, 5104 (2001).
- [30] I. M. Pop, K. Hasselbach, O. Buisson, W. Guichard, B. Pannetier, and I. Protodopov, Measurement of the current-phase relation in Josephson junction rhombi chains, *Phys. Rev. B* **78**, 104504 (2008).
- [31] A. Radosavljević, G. Gligorić, P. P. Beliĉev, A. Maluckov, and M. Stepić, Light propagation in binary Kagome ribbons with evolving disorder, *Phys. Rev. E* **96**, 012225 (2017).
- [32] M. Moratti, Transport phenomena in disordered time-dependent potentials, Ph.D. Thesis, Università degli Studi di Firenze, 2014.
- [33] T. Schwartz, G. Bartal, S. Fishman, and M. Segev, Transport and Anderson localization in disordered two-dimensional photonic lattices, *Nature* **446**, 52 (2007).
- [34] D. Leykam, S. Flach, O. Bahat-Treidel, and A. S. Desyatnikov, Flat band states: Disorder and nonlinearity, *Phys. Rev. B* **88**, 224203 (2013).

- [35] Y. Plotnik, M. A. Bandres, S. Stützer, Y. Lumer, M. C. Rechtsman, A. Szameit, and M. Segev, Analogue of Rashba pseudo-spin-orbit coupling in photonic lattices by gauge field engineering, *Phys. Rev. B* **94**, 020301(R) (2016).
- [36] D. Leykam, M. C. Rechtsman, and Y. D. Chong, Anomalous Topological Phases and Unpaired Dirac Cones in Photonic Floquet Topological Insulators, *Phys. Rev. Lett.* **117**, 013902 (2016).